Liquid Crystals
Publication details, including instructions for authors and subscription information:
http://www.informaworld.com/smpp/title~content=t713926090

Ferroelectric liquid crystals induced by dopants with axially chiral 2,2'-spirobiindan-1,1'-dione cores: diether vs. diester side-chains

Jeremy G. Finden[a]; Eagranie Yuh[a]; Christa Huntley[a]; Robert P. Lemieux[a]
[a] Chemistry Department, Queen's University, Ontario, K7L 3N6, Canada

To cite this Article Finden, Jeremy G. , Yuh, Eagranie , Huntley, Christa and Lemieux, Robert P.(2007) 'Ferroelectric liquid crystals induced by dopants with axially chiral 2,2'-spirobiindan-1,1'-dione cores: diether vs. diester side-chains', Liquid Crystals, 34: 9, 1095 — 1106
To link to this Article: DOI: 10.1080/02678290701528899
URL: http://dx.doi.org/10.1080/02678290701528899

Liquid Crystals, Vol. 34, No. 9, September 2007, 1095–1106

Ferroelectric liquid crystals induced by dopants with axially chiral 2,2′-spirobiindan-1,1′-dione cores: diether vs. diester side-chains

JEREMY G. FINDEN, EAGRANIE YUH, CHRISTA HUNTLEY and ROBERT P. LEMIEUX*
Chemistry Department, Queen's University, Kingston, Ontario, K7L 3N6, Canada

(*Received 26 April 2007; accepted 2 June 2007*)

A series of axially chiral 5,5′- and 6,6′-dialkanoyloxy-2,2′-spirobiindan-1,1′-dione dopants, (*R*)-**2** and (*R*)-**4a**–**4c** were synthesized in optically pure form and their ferroelectric polarization powers, δ_p, measured in four liquid crystal hosts with isotropic (I)–nematic (N)–smectic A (SmA)–smectic C (SmC) phase sequences. The results show that the sign of polarization P_S induced by (*R*)-**2** and (*R*)-**4a**–**4c** follows the same trend as that previously reported for the 5,5′- and 6,6′-diheptyloxy-2,2′-spirobiindan-1,1′-dione dopants, (*R*)-**1** and (*R*)-**3**. The polarization induced by (*R*)-**2** in the host **DFT** is below detection limits, and the sign of P_S was found to invert as a function of temperature at mole fractions as low as 0.01. On the other hand, the polarization power of the 6,6′-diheptanoyloxy dopant (*R*)-**4b** in the host **NCB76** is $-1449\,\mathrm{nC\,cm^{-2}}$, the fourth highest value reported so far, and more than three times the δ_p value of the 5,5′-diheptanoyloxy analogue (*R*)-**2** in that host ($+474\,\mathrm{nC\,cm^{-2}}$). Results of ^{2}H NMR experiments suggest that (*R*)-**4b** exerts stronger local perturbations in **NCB76** than (*R*)-**2**, and that these perturbations may be chiral in nature.

1. Introduction

Polar order in chiral smectic C (SmC*) liquid crystals formed by calamitic (rod-shaped) molecules arises from a combination of (i) rotational order about molecular long axes due to the uniform tilt of the SmC* layer and (ii) the chirality of constituent molecules, which results in a preferred orientation of any dipole coupled to the stereogenic centre along the polar C_2 axis of each SmC* layer [1–3]. Another macroscopic manifestation of molecular chirality in the SmC* phase is its helical structure, which causes the P_S vector to rotate from one layer to the next and results in zero polarization over a full helical pitch. However, the SmC* helix can be suppressed by confining the liquid crystal between parallel-rubbed polyimide coated glass slides with a spacing on the order of the helical pitch, thus producing a surface-stabilized ferroelectric state (SSFLC) with a net spontaneous polarization oriented perpendicular to the plane of the glass slides [4]. Coupling of the polarization with an alternating electric field on the order of volts per micron produces a fast-switching electro-optical light valve that is currently used in commercial high-resolution reflective liquid crystal microdisplays [5, 6], and that holds significant potential in nonlinear optics and photonics applications [7–10].

Ferroelectric SmC* materials used in commercial applications normally consist of an achiral liquid crystal host doped with a chiral additive (dopant) that may or may not be liquid crystalline. Because the performance characteristics of SSFLC devices often depends on the magnitude of P_S, a key aspect of FLC materials research is to understand the relationship between the molecular structure of a chiral dopant and the magnitude of the spontaneous polarization it induces [11, 12]. This relationship is expressed in terms of the polarization power δ_p according to [13],

$$\delta_p = \left(\frac{dP_o(x_d)}{dx_d}\right)_{x_d \to 0} \quad (1)$$

where x_d is the mole fraction of chiral dopant and P_o is the polarization normalized for variations in tilt angle θ according to [14].

$$P_o = P_S/\sin\,\theta. \quad (2)$$

The spontaneous polarization is a chiral property; it is either left-handed (negative) or right-handed (positive) depending on the absolute configuration of the chiral dopant. At the microscopic level, the origins of P_S can be understood in terms of asymmetric conformational energy profiles for polar functional groups sterically coupled to the stereogenic centre. Empirical and semiempirical structure–property relationships

*Corresponding author. Email: lemieux@chem.queensu.ca

Liquid Crystals
ISSN 0267-8292 print/ISSN 1366-5855 online © 2007 Taylor & Francis
http://www.tandf.co.uk/journals
DOI: 10.1080/02678290701528899

based on conformational analyses of such stereo-polar units are well established for dopants with chiral side-chains, which represent the vast majority of chiral dopants found in SmC* formulations [15–17]. In general, the polarization power of these compounds is invariant with respect to the structure of the liquid crystal host, which is consistent with the Boulder model for the molecular origins of P_S. According to this model, the SmC phase is considered to be a supramolecular host, and the conformational and orientational ordering of a chiral dopant is modelled by a mean field potential which qualitatively behaves like a binding site analogous to that described in host-guest chemistry [16, 17]. The binding site is C_{2h} symmetric and has a zigzag shape that is assumed to be invariant with respect to the host structure. To a first approximation, the Boulder model assumes that a chiral dopant plays the role of a 'passive' guest which adopts a conformation that best fits the achiral binding site of the SmC host.

Less conventional dopants with chiral cores induce spontaneous polarizations that tend to vary significantly with the structure of the SmC host [11, 12, 18]. For example, dopants with atropisomeric biphenyl cores exhibit remarkably high polarization powers in achiral SmC hosts with complementary phenylpyrimidine cores that enable the propagation of chiral perturbations via core–core interactions; such perturbations have been shown to enhance the polar order of the dopant as a feedback effect [19, 20]. This host effect may be viewed as a manifestation of molecular recognition with the host molecules that cannot be achieved with conventional dopants due to the higher degree of conformational disorder among side-chains in the diffuse layer structure of the SmC phase, i.e. the assumption of a shape invariance for the binding site in the original Boulder model appears to break down.

More recently, we reported on a new class of chiral dopants with an axially chiral 2,2′-spirobiindan-1,1′-dione core (see scheme 1), and showed that the variation in δ_p with the structure of the liquid crystal host may be explained in terms of an equilibrium between zigzag conformations of opposite polarities that have different steric demands in the core region of the binding site [21]. The polarization power of the 5,5′-diheptyloxy dopant (*R*)-**1** is uniformly positive in four different liquid crystal hosts (figure 1); it ranges from $+749\,\mathrm{nC\,cm^{-2}}$ in the host **PhP** to $+21\,\mathrm{nC\,cm^{-2}}$ in **DFT** at 10 K below the Curie point ($T - T_C = -10$ K). On the other hand, the polarization power of the 6,6′-diheptyloxy isomer (*R*)-**3** is uniformly negative; it ranges from $-79\,\mathrm{nC\,cm^{-2}}$ in **PhB** to $-1037\,\mathrm{nC\,cm^{-2}}$ in **NCB76** at $T - T_C = -10$ K. An analysis of zigzag conformations that conform to the binding site of the Boulder model

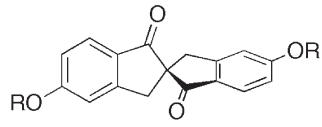

(*R*)-**1**, R = C_7H_{15}
(*R*)-**2**, R = $C(O)C_6H_{13}$

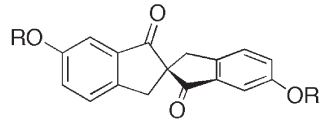

(*R*)-**3**, R = C_7H_{15}
(*R*)-**4**, R = $C(O)C_nH_{2n+1}$:
a, n=3; **b**, n=6; **c**, n=9

Scheme 1. Chemical structures of compounds **1**–**4**.

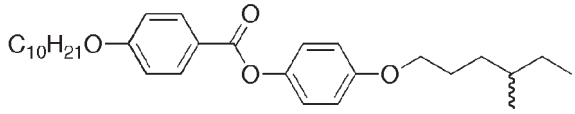

PhB: Cr 35 SmC 70.5 SmA 72 N 75 I

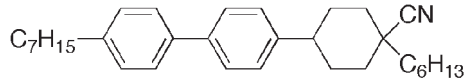

NCB76: Cr 66 (SmG 55) SmC 73 SmA 117 N 125 I

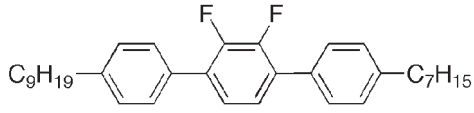

DFT: Cr 49 SmC 77 SmA 93 N 108 I

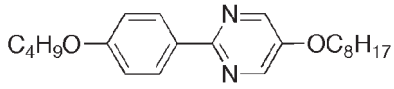

PhP: Cr 58 SmC 85 SmA 95 N 98 I

Figure 1. Liquid crystal host structures and phase transition temperatures (in °C).

suggests that the conformational distribution of both **1** and **3** in the SmC* phase may be described by two conformations with opposite dipole moments along the polar axis, as shown in figure 2 for dopant (*R*)-**1**. A correlation of the sign of P_S with the absolute configuration of each dopant according to this model suggests that the P conformer is favoured over the C_2 conformer in the SmC* phase, and that the variation in δ_p with the host structure may be explained by a shift in

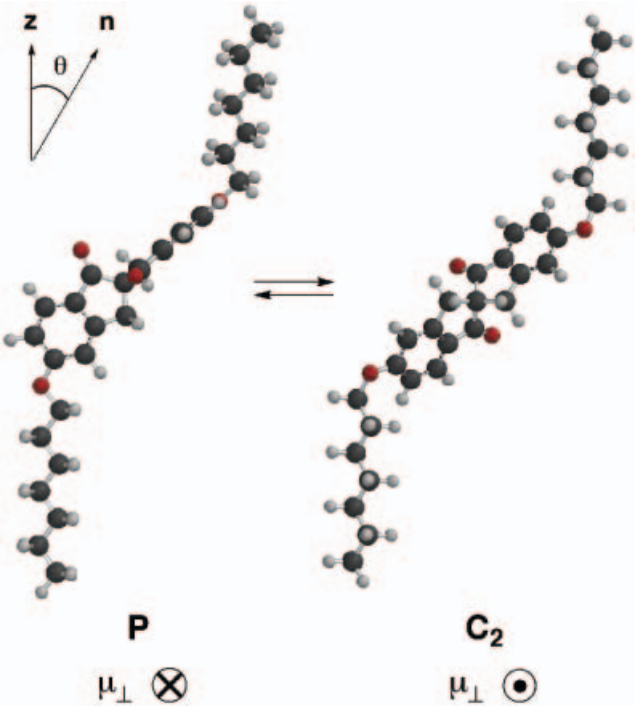

Figure 2. Molecular models showing the AM1-minimized zigzag conformations P and C_2 of dopant (*R*)-**1** as side-on views. The orientation of the transverse dipole moment $\mu_\perp$ along the polar axis is from negative to positive according to the physics convention.

the P/C_2 conformational distribution towards the C_2 conformer as the core section of the host binding site increases in length (from 9.7 Å for **PhP** to 14.4 Å for **DFT**). This is consistent with an estimated difference of ca. 1.5 Å in core section length between the P and C_2 conformers.

According to this model, a change in functional groups linking the paraffinic side-chains to the core should affect the conformational distribution of the dopant in the binding site of the host, and thus polar order, as well as the net transverse dipole moment of each contributing conformer. To test this hypothesis, we have modified the linking groups from ethers to esters and synthesized the 5,5′- and 6,6′-dialkanoyloxy analogues (*R*)-**2** and (*R*)-**4a–4c** in optically pure form. According to DFT-level conformational analyses of the rotation about the linking C–O bond in the model compounds 5-methoxy-1-indanone and 5-acetoxy-1-indanone (figure 3), the conformational distribution of the diesters (*R*)-**2** and (*R*)-**4a-c** in the binding site of a SmC host should be far more complex than that of the corresponding diethers, which might result in a 'dampening' of polar order. In this paper, we report measurements of δ_p values for (*R*)-**2** and (*R*)-**4a–4c** in the four liquid crystal hosts shown in figure 1, as well as

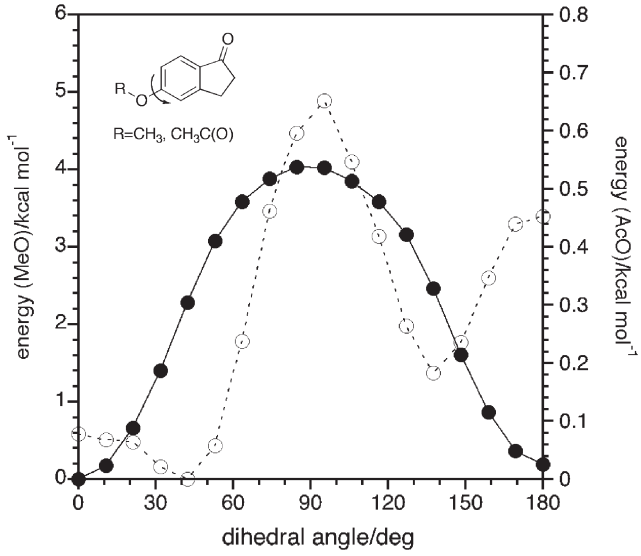

Figure 3. Relative energy profiles for 5-methoxy-1-indanone (filled circles) and 5-acetoxy-1-indanone (open circles) as a function of the dihedral angle defined by C(Me), O, C-5, and C-6, and C(C=O), O, C-5 and C-6, respectively, according to B3LYP/6-31G* calculations.

^{2}H NMR spectroscopy results suggesting that the 6,6′-diesters (*R*)-**4a-c** exert local perturbations in the host **NCB76** that may be chiral in nature.

2. Results and discussion

2.1. *Synthesis*

The 5,5′- and 6,6′-diester dopants **2** and **4a-c** were synthesized as racemic mixtures by condensation of 5,5′- and 6,6′-dihydroxy-2,2′-spirobiindan-1,1′-dione [21] with the required carboxylic acid using DCC and DMAP in yields ranging from 49 to 87%. The enantiomers were resolved by preparative chiral phase HPLC using a Daicel Chiralpak AS column, and recrystallized from hexanes prior to doping in the liquid crystal hosts. In each case, the absolute configuration of the first HPLC eluant was assigned as (*R*) based on a comparison of its CD spectrum with that of the corresponding (*R*)-diether, also the first eluant on the Chiralpak AS column (see appendix). The absolute configurations of the 5,5′-and 6,6′-diethers were previously assigned by the exciton chirality method [21].

2.2. *Dopant–host compatibility*

Compounds (*R*)-**2** and (*R*)-**4a–4c** were doped into the four liquid crystal hosts shown in figure 1, which exhibit isotropic (I)–nematic (N)–smectic A (SmA)–SmC phase sequences. Solubility limits were estimated by polarized microscopy based on the observation of persistent

biphasic SmC*/isotropic domains at 10 K below the Curie point of each mixture. The 5,5′-diester has an apparent solubility limit of ca. 20 mol. % in **NCB76**, 15 mol. % in **PhP** and **PhB** and 7.5 mol. % in **DFT**. Phase diagrams of these mixtures show a broadening of the N* phase and a depression of the SmA*–SmC* phase transition temperature with increasing dopant mole fraction x_d except in the case of **NCB76**, in which the addition of (*R*)-**2** results in a stabilization of the SmC* phase, as shown in figure 4a. As previously observed with the corresponding diethers, the 6,6′-diesters have significantly lower solubility limits than the 5,5′-diester; the solubility limits of (*R*)-**4a–4c** are below 5 mol. % in **PhP**, **PhB** and **DFT**, and range from 8 to 10 mol. % in **NCB76**. Phase diagrams for the **NCB76** mixtures show similar profiles to that obtained with (*R*)-**2** (figure 4b), including a stabilization of the SmC* phase with increasing dopant mole fraction. These results suggest that the binding site of **NCB76** provides a relatively good fit for dopants **2** and **4**.

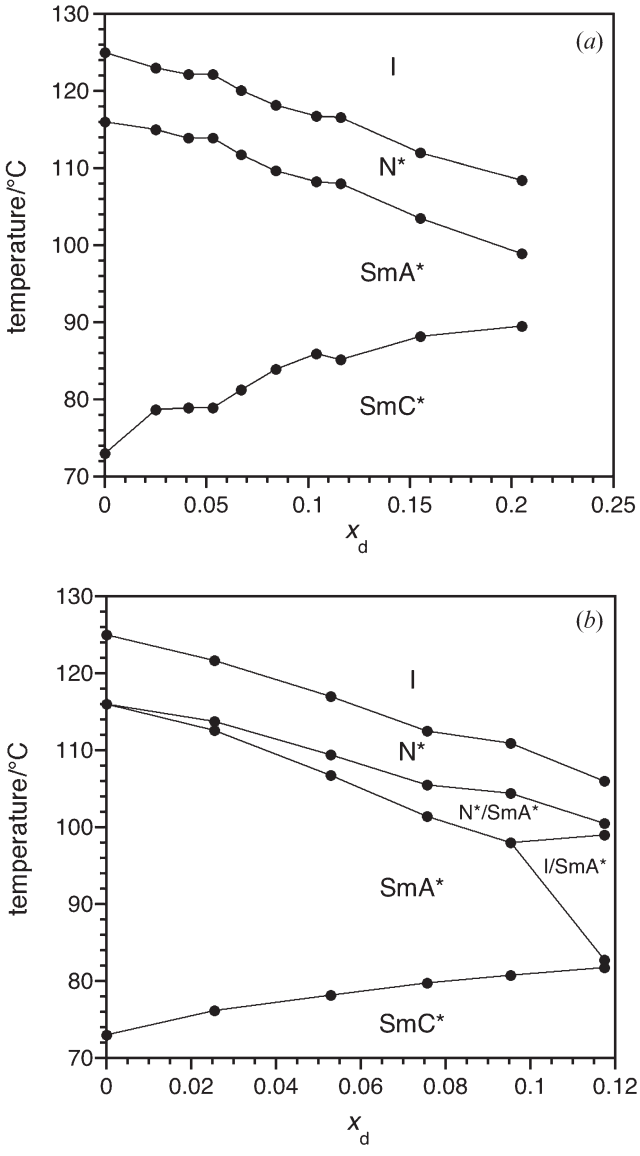

Figure 4. Partial phase diagrams of (a) (*R*)-**2** in **NCB76** and (b) (*R*)-**4c** in **NCB76**. The phase transition temperatures were measured on cooling by polarized microscopy.

2.3. *Polarization power measurements*

Homogeneous mixtures of the chiral dopants in the four liquid crystal hosts were aligned as SSFLC films using commercial ITO glass cells with rubbed polyimide surfaces and a cell gap of $4 \pm 0.5\,\mu m$. Spontaneous polarizations P_S and tilt angles θ were measured in the SmC* phase at $T - T_C = -10$ K by the triangular wave method [22]. The corresponding P_o values were calculated using equation (2) and plotted as a function of the dopant mole fraction x_d (see appendix). Linear $P_o(x_d)$ plots were obtained for mixtures of (*R*)-**2** in **PhP** and **PhB** up to the dopant solubility limit; the $P_o(x_d)$ plot obtained for mixtures of (*R*)-**2** in **NCB76** is linear up to $x_d = 0.12$, but levels off at higher mole fractions, which is likely due to a saturation of the SmC* phase and a partitioning of the dopant between smectic and isotropic liquid microdomains that could not be detected by polarized microscopy. The polarization induced by (*R*)-**2** in **DFT** was below the detection limit of our instrument ($0.3\,nC\,cm^{-2}$) up to the dopant solubility limit of $x_d = 0.075$, and δ_p is therefore reported as an upper limit. Each $P_o(x_d)$ plot (or the linear portion of the $P_o(x_d)$ plot in the case of the **NCB76** mixtures) gave a good least-squares fit from which the δ_p value was derived, according to equation 1 (table 1).

As shown in figure 5, the polarization power of (*R*)-**2** is uniformly positive at $T - T_C = -10$ K in all four hosts, which is consistent with the polarization power data previously reported for the diheptyloxy analogue (*R*)-**1**. The δ_p values in **PhB** and **PhP** are 50–60% lower than for (*R*)-**1**, but δ_p is 30% higher in **NCB76**, which may reflect the difference in conformational energy profiles between the two linking groups. In **DFT**, the sign of P_S induced by (*R*)-**2** inverts from positive to negative with decreasing temperature. This phenomenon is invariant of x_d, except for a decrease in the reduced inversion temperature $T_{inv} - T_C$ with increasing dopant mole fraction, from 25 K at $x_d = 0.01$ to 16 K at $x_d = 0.075$. Electro-optical measurements of the tilt angle θ as a function of temperature gave profiles typical of FLC materials with a second order SmA*–SmC* phase transition except for a discontinuity at the P_S inversion temperature, at which no Goldstone-mode switching could be detected (figure 6).

Table 1. Polarization powers δ_p of (*R*)-**2** and (R)-**4a-c** in the hosts **PhP**, **PhB**, **NCB76** and **DFT** at $T - T_C = -10$ K.

	δ_p/nC cm^{-2} [a,b]			
Dopant	**PhP**	**PhB**	**NCB76**	**DFT**
(*R*)-**2**	315 ± 26 (+)	242 ± 24 (+)	474 ± 44 (+)	<30 (+/−)[c]
(*R*)-**4a**	<30 (−)	>120 (−)	1389 ± 51 (−)	(−)[d]
(*R*)-**4b**	<39 (−)	>97 (−)	1449 ± 36 (−)	(−)[d]
(*R*)-**4c**	<27 (−)	>150 (−)	1213 ± 68 (−)	>240 (−)

[a]Sign of polarization in parentheses. [b]Uncertainty is ± standard error of least-squares fit. [c]Inversion of polarization with temperature. [d]Dopants crystallized above the Curie point.

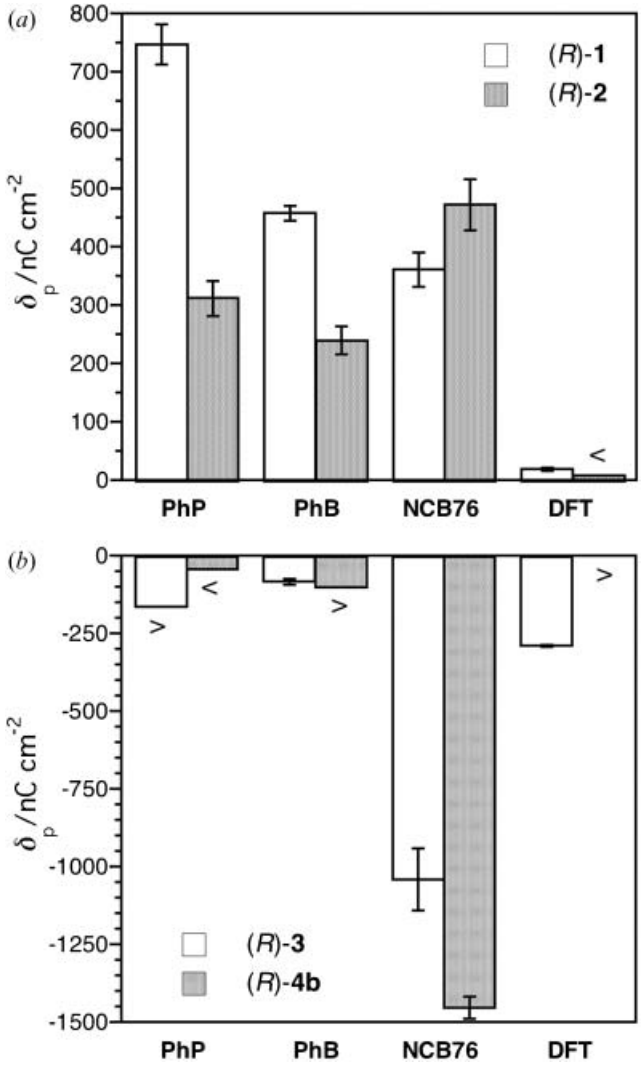

Figure 5. Bar graphs showing a comparison of polarization power values δ_p between dopants (*R*)-**1** and (*R*)-**2** (left) and between dopants (*R*)-**3** and (*R*)-**4b** (right) at $T - T_C = -10$ K in the liquid crystal hosts **PhP**, **PhB**, **NCB76** and **DFT**. The < sign indicates an upper limit value based on the instrument detection limit of 0.3 nC cm^{-2}, whereas the > sign indicates a lower limit based on the observation of persistent SmC–I phase separation at $T - T_C = -10$ K.

Observations of polarization inversion as a function of temperature have been reported previously for induced SmC* mixtures with dopant mole fractions that are considerably higher than 1 mol. % [23–25]. In such cases, the inversion of polarization was attributed to a shift in balance between dopant–host and dopant–dopant interactions contributing to polarizations of opposite signs. Given that the inversion of P_S reported herein occurs with dopant mole fractions as low as 1 mol. %, which precludes any significant dopant-dopant interactions, an alternative rationale is required. Goodby and co-workers reported an inversion of polarization as a function of temperature for a series of chiral (*S*)-2-methylbutyl 4-*n*-alkanoyloxybiphenyl-4′-carboxylate mesogens, and proposed that the inversion may result from a shift in the distribution of conformational and/or rotational states of opposite polarities

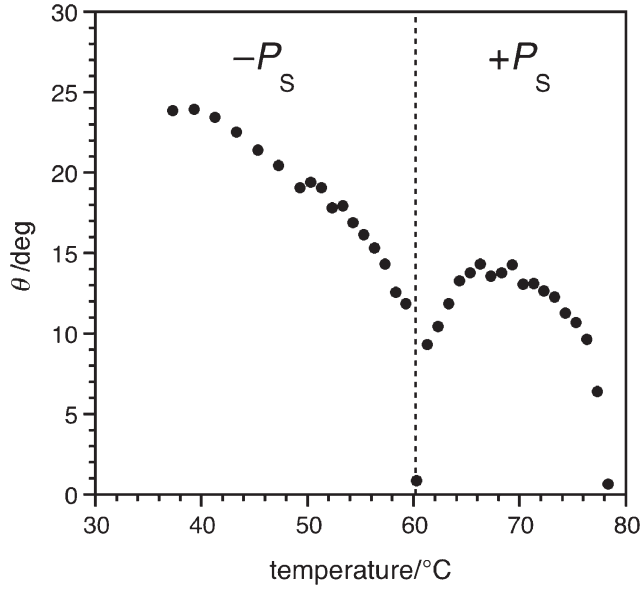

Figure 6. Electro-optical tilt angle θ as a function of temperature for a 4.9 mol. % mixture of (*R*)-**2** in **DFT** aligned in a 4 μm ITO glass cell with rubbed polyimide surfaces. The polarization inversion temperature is indicated by the dotted line.

[26]. This explanation is entirely plausible in the present case considering that the spontaneous polarization is below detection limit, which suggests a delicate balance between conformers of opposite polarities that can be shifted in either direction by a small perturbation such as a change in temperature.

Linear $P_o(x_d)$ plots were obtained for mixtures of (*R*)-**4a-c** in **NCB76** up to the dopant solubility limits, and gave very good least-squares fits. The resulting δ_p values for (*R*)-**4a** and **-4b** are not statistically different at the 95% confidence level, whereas the lower δ_p value for the dopant (*R*)-**4c** may reflect a more complex conformational hypersurface due to the longer side-chains, which could have a small dampening effect on polar order [27]. The δ_p value of $-1449\,nC\,cm^{-2}$ recorded for (*R*)-**4b** in **NCB76** is 40% higher than that reported for the 6,6′-diheptyloxy dopant (*R*)-**3**, and is near the record value of $-1738\,nC\,cm^{-2}$ reported for the axially chiral biphenyl dopant (*R*)-**5** (scheme 2) in **PhP** [19]. The polarization induced by (*R*)-**4a–4c** in **PhP** was below the detection limit of our instrument up to the dopant solubility limit. The δ_p values reported for mixtures of (*R*)-**4a–4c** in **PhB** are given as lower limits due to the persistence of isotropic domains in the SmC* phase at $T - T_C = -10$ K. The polarization power of (*R*)-**4c** in **DFT** is also given as a lower limit due to the partial crystallization of the dopant in the SmC* phase at $T - T_C = -10$ K; the shorter chain homologues (*R*)-**4a** and **-4b** started to crystallize above the Curie point and no polarization could be measured. Nevertheless, Goldstone-mode switching was observed in all cases, and the polarization induced by the 6,6′-dialkanoyloxy dopants is uniformly negative in all hosts, which is consistent with the δ_p data reported for the 6,6′-dialkoxy analogue (*R*)-**3** [21].

The poor compatibility of the 6,6′-diheptanoyloxy dopant (*R*)-**4b** with three of the four liquid crystal hosts makes it difficult to draw useful comparisons between its δ_p values and those of the corresponding 5,5′-diheptanoyloxy dopant (*R*)-**2**, except in **NCB76**. In that liquid crystal host, the dependence of δ_p on the position of the heptanoyloxy side-chains is very similar to that observed for the diheptyloxy dopants (*R*)-**1** and (*R*)-**3**, i.e. we observe a 3.2-fold increase in the absolute value of δ_p going from the 5,5′- to the 6,6′-diheptanoyloxy dopant vs. a 2.8-fold increase going from the 5,5′- to the 6,6′-diheptyloxy dopant. In the latter case, the increase in δ_p was rationalized according to the P/C_2 conformational distribution model (figure 2) based on two factors: (i) an increase in transverse dipole moment of the P conformer (+1.6 D for (*R*)-**1** vs. −3.5 D for (*R*)-**3**), and (ii) a greater propensity of the 6,6′-diheptyloxy dopant to exert local chiral perturbations on the SmC host (vide infra), which could shift the conformational equilibrium as a feedback effect [21].

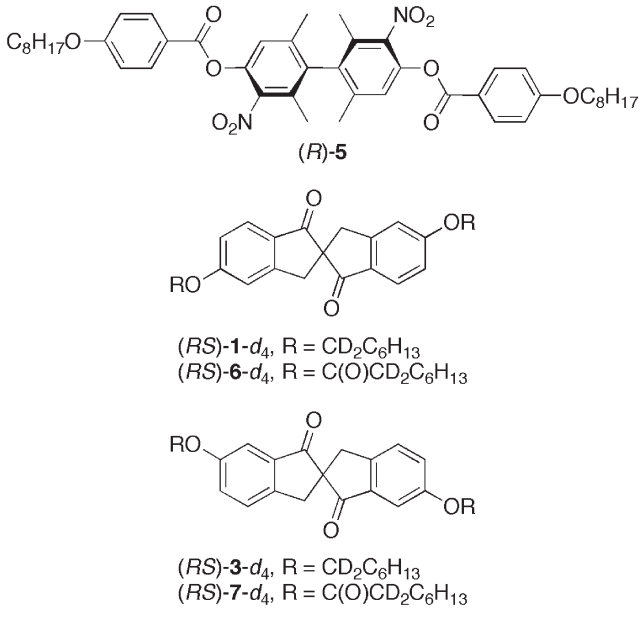

Scheme 2. Chemical structures of compounds **5–7**.

2.4. *^{2}H NMR Spectroscopy*

^{2}H NMR spectroscopy was used to investigate the effect of varying the positions of the ester side-chains on local ordering in the host **NCB76**. In an anisotropic fluid, the interaction of the quadrupolar moment of a deuterium nucleus with the electric field gradient tensor produces a quadrupolar doublet with a splitting $\Delta\nu_Q$ that is directly proportional to the orientational order parameter of the C–D bond. In a previous study [21], we reported the ^{2}H NMR spectra of the racemic diheptyloxy dopants (*RS*)-**1**-d_4 and (*RS*)-**3**-d_4 in the SmC phase of **NCB76**. As shown in figure 7, the ^{2}H NMR spectrum of (*RS*)-**1**-d_4 in **NCB76** at $T - T_C = -10$ K features one quadrupolar doublet with $\Delta\nu_Q = 58$ kHz, which indicates that all dopant molecules reside in a smectic liquid crystalline environment. On the other hand, the ^{2}H NMR spectrum of (*RS*)-**3**-d_4 in **NCB76** obtained under the same conditions features two quadrupolar doublets with $\Delta\nu_Q = 56$ and 28 kHz ($\Delta\Delta\nu_Q = 28$ kHz). Control experiments confirmed that the two doublets are not indicative of a partitioning of the dopant molecules between two different anisotropic phases. Instead, we proposed that the pair of quadrupolar doublets results from a *local* chiral perturbation of **NCB76** that causes the methylene deuterons to become non-equivalent [28], a phenomena that had been previously observed with the enantiotropic methylene deuterons of achiral dopants dissolved in the chiral nematic phase formed

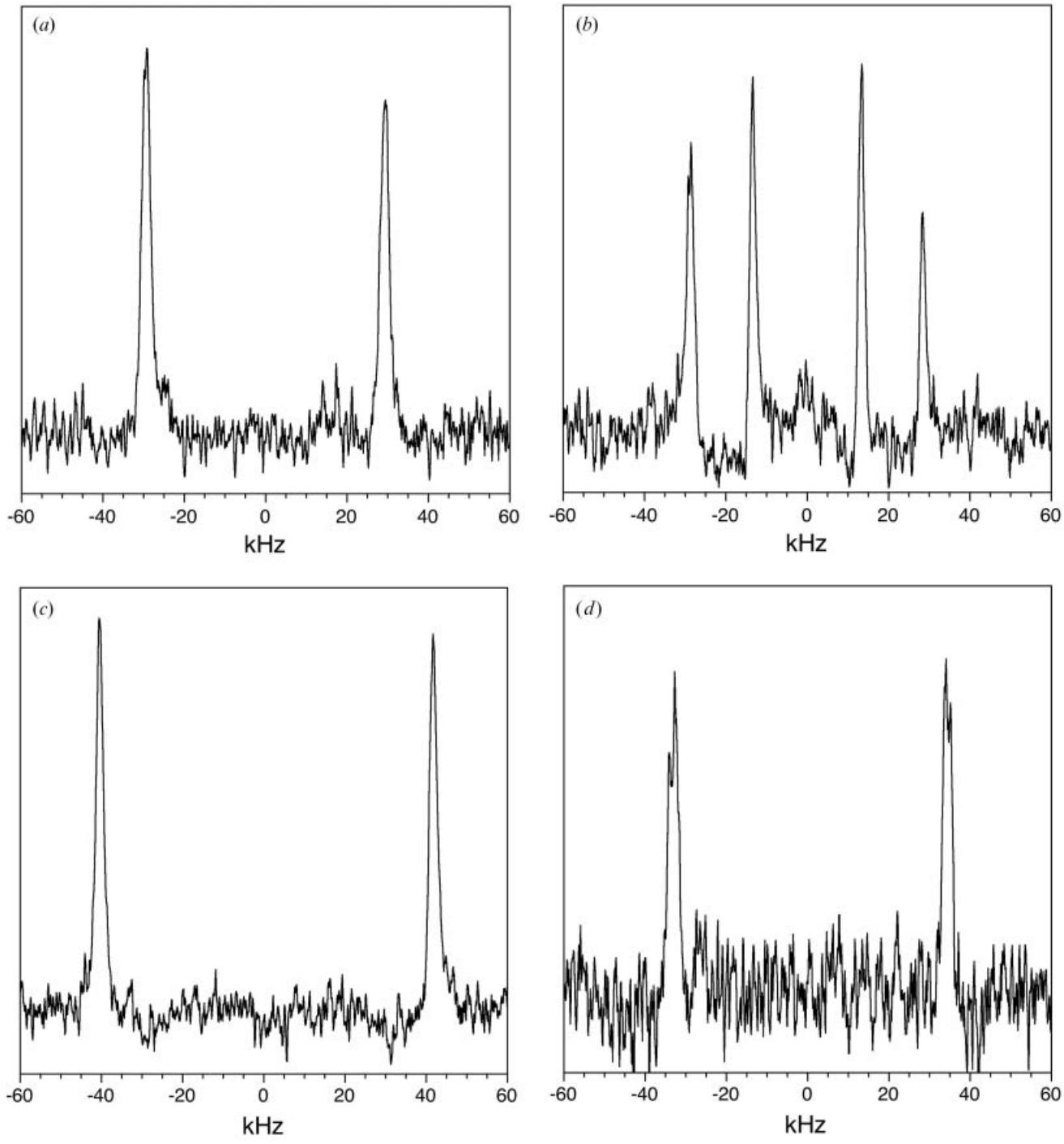

Figure 7. ^{2}H NMR spectra (92 MHz) of four deuterated dopants in the liquid crystal host **NCB76** taken at $T - T_C = -10$ K: (a) (*RS*)-**1**-d_4, 10 mol. %; (b) (*RS*)-**3**-d_4, 5 mol. %; (c) (*RS*)-**6**-d_4, 5 mol. %; (d) (*RS*)-**7**-d_4, 5 mol. %.

by solutions of poly-γ-benzyl-L-glutamate (PBLG) [29, 30].

We carried out similar ^{2}H NMR experiments with the racemic diester dopants (*RS*)-**6**-d_4 and (*RS*)-**7**-d_4 (see scheme 2), which feature deuterated octanoyloxy side-chains derived from the commercially available octanoic-2,2-d_2 acid. As shown in figure 7, the ^{2}H NMR spectrum of the 5,5′-diester (*RS*)-**6**-d_4 in **NCB76** features one doublet with a quadrupolar splitting $\Delta\nu_Q$ of 82 kHz, which is significantly larger than the quadrupolar splitting of 68 kHz observed with the 6,6′-diester (*RS*)-**7**-d_4 under the same conditions. This

indicates a reduction in orientational order of the C–D bonds that may result from a stronger local perturbation exerted by the 6,6′-diester on the liquid crystal host. Interestingly, we also observe a splitting $\Delta\Delta\nu_Q$ of the quadrupolar doublet in the (*RS*)-**7**-d_4 spectrum of ca. 3 kHz, which suggests that the local perturbation may be chiral in nature. The splitting $\Delta\Delta\nu_Q$ is much smaller than that observed with the 6,6′-diether (*RS*)-**3**-d_4, which may be due, in part, to the fact that the methylene deuterons are further removed from the stereogenic centre.

3. Conclusions

The polarization powers δ_p of a series of axially chiral 5,5′- and 6,6′-dialkanoyloxy-2,2′-spirobiindan-1,1′-dione dopants, (*R*)-**2** and (*R*)-**4a–4c**, were measured in four liquid crystal hosts with I–N–SmA–SmC phase sequences and compared to δ_p values previously reported for the corresponding dialkoxy dopants (*R*)-**1** and (*R*)-**3**. The results show that the sign of polarization induced by (*R*)-**2** and (*R*)-**4a–4c** follows the same trend as that reported for (*R*)-**1** and (*R*)-**3**. However, changing the linking groups from ethers to esters resulted in changes in δ_p values that may reflect a significant difference in the conformational energy profiles of the two linking groups. These results, including the observation of polarization sign inversion as a function of temperature at low dopant mole fractions, are consistent with a conformational distribution model originally proposed for the polar ordering of the dialkoxy dopants (*R*)-**1** and (*R*)-**3**. Furthermore, the results of ^{2}H NMR experiments suggest that the 6,6′-diester dopant exerts stronger local perturbations in **NCB76** than the corresponding 5,5′-diester dopant, and that these perturbations may be chiral in nature. Such local chiral perturbations may be responsible, at least in part, for the high polarization powers of the 6,6′-diester dopants in **NCB76** according to the chirality transfer feedback mechanism postulated in previous studies [19, 20] Indeed, the polarization power of (*R*)-**4b** in **NCB76** is the fourth highest value reported heretofore [19, 31].

4. Experimental

4.1. *Synthesis*

4.1.1. (*R*)- and (*S*)-5,5'-Diheptoyloxy-2,2'-spirobiindan-1,1'-dione ((*R*)-2 and (*S*)-2). Under an argon atmosphere, DCC (259 mg, 1.25 mmol) was added to a stirred solution of (*RS*)-5,5′- dihydroxy-2,2′-spirobiindan-1,1′-dione [21] (100 mg, 0.36 mmol), DMAP (153 mg, 1.25 mmol) and heptanoic acid (163 mg, 1.25 mmol) in dry CH_2Cl_2 (5 ml). The solution was stirred at room temperature overnight, then filtered, concentrated and the residue taken up in EtOAc. The organic extract was washed with 2% aq HCl, dried ($MgSO_4$) and concentrated. The residue was purified by flash chromatography on silica gel (15% EtOAc/hexanes) to give 89 mg (49%) of (*RS*)-**2** as a white solid, m.p. 108–110°C. ^{1}H NMR (400 MHz, $CDCl_3$): δ 7.76 (d, J=8 Hz, 2H), 7.30 (d, J=2 Hz, 2H), 7.12 (dd, J=8 Hz, 2 Hz, 2H), 3.89 (d, J=17 Hz, 2H), 3.18 (d, J=17 Hz, 2H), 2.59 (t, J=7 Hz, 4H), 1.76 (quintet, J=7 Hz, 4H), 1.32–1.46 (m, 12H), 0.91 (t, J=7 Hz, 6H). ^{13}C NMR (75 MHz, $CDCl_3$): δ 14.0, 22.5, 24.8, 28.7, 31.4, 34.4, 37.9, 65.6, 119.4, 122.0, 126.2, 132.8, 155.5, 156.5, 171.7, 210.1. MS (TOF-MS) m/z 504 (M^+): HRMS (TOF-MS) calculated for $C_{31}H_{36}O_6$, 504.2512; found, 504.2512. UV (hexanes): λ_{max} ($\log\varepsilon$) 207 (4.72), 256 (4.56), 283 (4.17), 292 (4.13). The racemic mixture was resolved by preparative chiral phase HPLC using a Daicel Chiralpak AS column (50 cm × 5 cm i.d., 10% EtOH in hexanes, 50 ml min^{-1}) to give (*R*)-**2** and (*S*)-**2** (first and second eluants, respectively) in optically pure form: CD ((*R*)-**2,** hexanes): λ_{ext} ($\Delta\varepsilon$) 200 (16.1), 211 (−35.8), 220 (2.5), 223 (−0.7), 225 (0.7), 234 (11.2), 237 (11.4), 248 (−6.9), 263 (2.8), 294 (−7.5), 306 (−0.2), 327 (−2.6), 335 (−1.9), 339 (−3.4). Elemental analysis: calculated for $C_{31}H_{36}O_6$, C 73.79, H 7.19%; found, C 73.93, H 7.26%.

4.1.2. (*R*)- and (*S*)-6,6'-Dibutanoyloxy-2,2′-spirobiindan-1,1′-dione ((*R*)-4a and (*S*)-4a). The procedure used for the synthesis of (*RS*)-**2** was repeated with (*RS*)-6,6′-dihydroxy-2,2′-spirobiindan-1,1′-dione [21] (69 mg, 0.25 mmol) and butyric acid (0.07 ml, 0.74 mmol). Purification by flash chromatography on silica gel (30% EtOAc/hexanes) gave 76 mg (73%) of (*RS*)-**4a** as a white solid, m.p. 153–154°C. ^{1}H NMR (400 MHz, $CDCl_3$): δ 1.05 (t, J=7.3 Hz, 6H), 1.74–1.84 (m, 4H), 2.56 (t, J=7.3 Hz, 4H), 3.16 (d, J=17.2 Hz, 2H), 3.69 (d, J=17.2 Hz, 2H), 7.37 (d, J=8.3 Hz, 2H), 7.45 (s, 2H), 7.55 (d, J=8.3 Hz, 2H). ^{13}C NMR (100 MHz, $CDCl_3$): δ 13.8, 18.6, 36.3, 37.8, 66.7, 117.6, 127.2, 129.3, 136.7, 150.7, 151.0, 172.1, 201.6. MS (EI) m/z 420 (M+, 36), 350 (52), 280 (100), 252 (21), 71 (32). HRMS (EI): calculated for $C_{25}H_{24}O_6$, 420.1573; found, 420.1564. UV (hexanes) λ_{max} ($\log\varepsilon$): 207 (4.68), 248 (4.45), 290 (4.05). The enantiomers were resolved by chiral phase HPLC using a Daicel Chiralpak AS column (50 cm × 5 cm i.d., 30% EtOH in hexanes, 50 ml min^{-1}) to give (*R*)-**4a** and (*S*)-**4a** (first and second eluants, respectively) in optically pure form: CD ((*R*)-**4a**, hexanes) λ_{ext} ($\Delta\varepsilon$) 208 (−17.0), 215 (15.3), 222 (6.9), 230 (11.8), 246 (−7.0), 256 (2.8), 303 (−6.8), 323 (3.5), 330 (1.7), 337 (3.1), 345 (0.7), 351 (1.7), 366 (0.7), 377

(1.1). Elemental analysis: calculated for $C_{25}H_{24}O_6$, C 71.41, H 5.75%; found, C 71.37, H 6.15%.

4.1.3. (*R*)- and (*S*)-6,6′-Diheptanoyloxy-2,2′-spirobiindan-1,1′-dione ((*R*)-4b and (*S*)-4b). The procedure used for the synthesis of (*RS*)-**2** was repeated with (*RS*)-6,6′-dihydroxy-2,2′-spirobiindan-1,1′-dione [21] (76 mg, 0.27 mmol) and heptanoic acid (0.11 ml, 0.81 mmol). Purification by flash chromatography on silica gel (20% EtOAc/hexanes) gave 76 mg (55%) of (*RS*)-**4b** as a white solid, m.p. 104–105°C. ^{1}H NMR (400 MHz, $CDCl_3$): δ 0.91 (t, J=6.1 Hz, 6H), 1.25–1.45 (m, 12H), 1.70–1.80 (m, 4H), 2.57 (t, J=7.5 Hz, 4H), 3.17 (d, J=17.0 Hz, 2H), 3.70 (d, J=17.0 Hz, 2H), 7.37 (d, J=8.4 Hz, 2H), 7.45 (s, 2H), 7.55 (d, J=8.4 Hz, 2H). ^{13}C NMR (100 MHz, $CDCl_3$): δ 14.2, 22.6, 25.0, 28.9, 31.6, 34.4, 37.8, 66.7, 117.6, 127.3, 129.3, 136.7, 150.7, 151.0, 172.3, 201.6. MS (EI) m/z 504 (M+, 24), 392 (54), 280 (100), 252 (7), 113 (23), 85 (9). HRMS (EI): calculated for $C_{31}H_{36}O_6$, 504.2512; found, 504.2526. UV (hexanes) λ_{max} (log ε) 208 (4.69), 248 (4.47), 290 (4.04). The enantiomers were resolved by chiral phase HPLC using a Daicel Chiralpak AS column (50 cm × 5 cm i.d., 30% EtOH in hexanes, 50 ml min^{-1}) to give (*R*)-**4b** and (*S*)-**4b** (first and second eluants, respectively) in optically pure form. CD ((*R*)-**4b**, hexanes) λ_{ext} ($\Delta\varepsilon$): 208 (14.6), 215 (16.3), 222 (7.6), 231 (11.6), 247 (−7.0), 258 (2.7), 302 (−6.6), 324 (3.4), 331 (1.0), 337 (2.9), 345 (0.4), 353 (1.6), 361 (0.5), 367 (1.1), 392 (−0.2). Elemental analysis: calculated for $C_{31}H_{36}O_6$, C 73.79, H, 7.19%; found, C 73.62, H 7.04%.

4.1.4. (*R*)- and (*S*)-6,6′-Didecanoyloxy-2,2′-spirobiindan-1,1′-dione ((*R*)-4c and (*S*)-4c). The procedure used for the synthesis of (*RS*)-**2** was repeated with (*RS*)-6,6′-dihydroxy-2,2′-spirobiindan-1,1′-dione [21] (73 mg, 0.26 mmol) and decanoic acid (0.135 g, 0.78 mmol). Purification by flash chromatography on silica gel (20% EtOAc/hexanes) gave 133 mg (87%) of (*RS*)-**4c** as a white solid, m.p. 89–91°C; ^{1}H NMR (400 MHz, $CDCl_3$): δ 0.88 (t, J=7.1 Hz, 6H), 1.20–1.45 (m, 24H), 1.71–1.79 (m, 4H), 2.57 (t, J=7.6 Hz, 4H), 3.16 (d, J=17.1 Hz, 2H), 3.69 (d, J=17.1 Hz, 2H), 7.36 (d, J=8.3 Hz, 2H), 7.45 (s, 2H), 7.55 (d, J=8.3 Hz, 2H). ^{13}C NMR (100 MHz, $CDCl_3$): δ 14.2, 22.8, 25.0, 29.2, 29.4, 29.5, 32.0, 34.4, 37.8, 66.7, 117.6, 127.2, 129.3, 136.7, 150.7, 151.0, 172.2, 201.6. MS (EI) m/z 588 (M+, 9), 434 (36), 280 (100), 252 (18), 98 (22), 55 (36). HRMS (EI): calculated for $C_{37}H_{48}O_6$, 588.3451; found, 588.3452. UV (hexanes) λ_{max} (log ε): 207 (4.66), 248 (4.42), 291 (3.92). The enantiomers were resolved by chiral phase HPLC using a Daicel Chiralpak AS column (50 cm × 5 cm i.d., 10% EtOH in hexanes, 50 ml min^{-1}) to give (*R*)-**4c** and (*S*)-**4c** (first and second eluants, respectively) in optically pure form. CD ((*R*)-**4c**, hexanes): λ_{ext} ($\Delta\varepsilon$) 208 (–15.2), 215 (14.5), 222 (7.9), 231 (12.9), 246 (–5.7), 259 (4.2), 303 (–6.3), 324 (3.6), 331 (1.8), 337 (2.5), 345 (0.5), 352 (1.7), 362 (0.5), 370 (0.9), 375 (0.4), 381 (1.1), 388 (–0.1), 392 (0.3). Elemental analysis: calculated for $C_{37}H_{48}O_6$, C 75.48, H 8.22%; found, C 75.48, H 8.15%.

4.1.5. (*RS*)-5,5′-Bis(octanoyloxy-2,2-d_2)-2,2′-spirobiindan-1,1′-dione ((*RS*)-6-d_4). The procedure used for the synthesis of (*RS*)-**2** was repeated with (*RS*)-5,5′-dihydroxy-2,2′-spirobiindan-1,1′-dione [21] (0.11 g, 0.38 mmol) and octanoic-d_2-2,2 acid (0.30 ml, 1.15 mmol). Purification by flash chromatography on silica gel (33% EtOAc/hexanes) gave 110 mg (52 %) of (*RS*)-**6**-d_4 as a white solid, m.p. 117.5–118.5°C. ^{1}H NMR (300 MHz, $CDCl_3$): δ 7.77 (d, J=9 Hz, 2H), 7.30 (d, J=3 Hz, 2H), 7.12 (dd, J=3, 9 Hz, 2H), 3.69 (d, J=18 Hz, 2H), 3.18 (d, J=15 Hz, 2H), 1.75 (m, 4H), 1.31 (m, 16H), 0.89 (t, J=6 Hz, 6H). ^{13}C NMR (100 MHz, $CDCl_3$): δ 13.0, 21.6, 23.7, 23.8, 27.9, 28.0, 30.6, 36.9, 64.6, 118.3, 120.9, 125.2, 131.8, 154.5, 155.5, 170.7, 200.0. MS (TOF-MS) m/z 536 ([M]$^+$, 2), 409 (48), 282 (100), 281 (55). HRMS (TOF-MS): calculated for $C_{33}H_{36}D_4O_6$, 536.3076; found, 536.3089.

4.1.6. (*RS*)-6,6′-Bis(octanoyloxy-2,2-d_2)-2,2′-spirobiindan-1,1′-dione ((*RS*)-7-d_4). The procedure used for the synthesis of (*RS*)-**2** was repeated with (*RS*)-5,5′-dihydroxy-2,2′-spirobiindan-1,1′-dione [21] (50 mg, 0.18 mmol) and octanoic-2,2-d_2 acid (0.14 ml, 0.54 mmol). Purification by flash chromatography on silica gel (25% EtOAc/hexanes) gave 70 mg (70 %) of (*RS*)-**7**-d_4 as a white solid, m.p. 100–101°C. ^{1}H NMR (300 MHz, $CDCl_3$): δ 7.55 (d, J=9 Hz, 2H), 7.44 (d, J=3 Hz, 2H), 7.36 (dd, J=3, 9 Hz, 2H), 3.69 (d, J=18 Hz, 2H), 3.16 (d, J=18 Hz, 2H), 1.74 (m, 4H), 1.30 (m, 16H), 0.88 (t, J=6 Hz, 6H). ^{13}C NMR (100 MHz, $CDCl_3$): δ 14.0, 22.6, 24.8, 28.9, 29.0, 31.6, 37.7, 66.5, 117.5, 127.1, 129.2, 136.6, 150.6, 150.8, 172.1, 201.5. MS (TOF-MS): m/z 536 ([M]$^+$, 7), 409 (54), 282 (96), 281 (100). HRMS (TOF-MS): calculated for $C_{33}H_{36}D_4O_6$, 536.3076; found, 536.3093.

4.2. *Ferroelectric polarization measurements*

Texture analyses and transition temperature measurements for the doped liquid crystal mixtures were performed using either a Nikon Labophot-2 POL or Nikon Eclipse E600 POL polarized microscope fitted with a Linkam LTS 350 hot stage. Spontaneous polarizations (P_S) were measured as a function of temperature by the triangular wave method [22]

($6\,V\,\mu m^{-1}$, 80–100 Hz) using a Displaytech APT-III polarization testbed in conjunction with the Linkam hot stage. Parallel rubbed polyimide-coated ITO glass cells (4 μm spacing) supplied by E.H.C. Co. were used for the measurements. Good alignment was obtained by slow cooling of the filled cells from the isotropic phase via the N* and SmA* phases. Tilt angles (θ) were measured as a function of temperature between crossed polarizers as half the rotation between two extinction positions corresponding to opposite polarization orientations. The sign of P_S along the polar axis was assigned from the relative configuration of the electrical field and the switching position of the sample according to the established convention [16].

4.3. *^{2}H NMR experiments*

The ^{2}H NMR experiments were performed using a Bruker Avance 600 spectrometer (92.13 MHz). For each experiment, the samples were first heated to the isotropic phase, then cooled to the appropriate temperature and allowed to equilibrate for 10 min. The temperature control unit of the probe was calibrated using ethylene glycol in DMSO-d_6 following the standard procedure. The temperatures are considered accurate to within ± 1 K and could be controlled to within ± 0.1 K [32]. The spectra were recorded for stationary samples using a solid echo pulse sequence, collecting 4096 points per scan over a 250 kHz spectral width. For each spectrum in a liquid crystal phase, 175 999–738 398 scans were collected. Line broadening (250 Hz), exponential multiplication and iterative left-shifting of the data (which ensures the first data point of the FID coincides with the beginning of the echo decay) were carried out prior to Fourier transformation.

Acknowledgments

We are grateful to the Natural Sciences and Engineering Research Council of Canada and the Canada Foundation for Innovation for support of this work.

References

[1] D.M. Walba, S.C. Slater, W.N. Thurmes, N.A. Clark, M.A. Handschy, F. Supon. *J. Am. chem. Soc.*, **108**, 5210 (1986).
[2] J.W. Goodby, E. Chin, T.M. Leslie, J.M. Geary, J.S. Patel. *J. Am. chem. Soc.*, **108**, 4729 (1986).
[3] D.J. Photinos, E.T. Samulski. *Science*, **270**, 783 (1995).
[4] N.A. Clark, S.T. Lagerwall. *Appl. Phys. Lett.*, **36**, 899 (1980).
[5] S.T. Lagerwall. *Ferroelectric and Antiferroelectric Liquid Crystals*. Wiley-VCH, Weinheim (1999).
[6] D.M. Walba. *Science*, **270**, 250 (1995).
[7] D.M. Walba, L. Xiao, P. Keller, R. Shao, D. Link, N.A. Clark. *Pure appl. Chem.*, **71**, 2117 (1999).
[8] W.A. Crossland, T.D. Wilkinson. In *Handbook of Liquid Crystals*, Vol. 1, D. Demus, J.W. Goodby, G.W. Gray, H.-W. Spiess, V. Vill (Eds), Wiley-VCH, Weinheim (1998).
[9] T. Ikeda, A. Kanazawa. In *Molecular Switches*, B.L. Feringa (Ed.), Wiley-VCH, Weinheim (2001).
[10] R.P. Lemieux. *Soft Matter*, **1**, 348 (2005).
[11] H. Stegemeyer, R. Meister, U. Hoffmann, A. Sprick, A. Becker. *J. Mater. Chem.*, **5**, 2183 (1995).
[12] R.P. Lemieux. *Accts Chem. Res.*, **34**, 845 (2001).
[13] K. Siemensmeyer, H. Stegemeyer. *Chem. Phys. Lett.*, **148**, 409 (1988).
[14] W. Kuczynski, H. Stegemeyer. *Chem. Phys. Lett.*, **70**, 123 (1980).
[15] J.W. Goodby. In *Ferroelectric Liquid Crystals: Principles, Properties and Applications*, J.W. Goodby, R. Blinc, N.A. Clark, S.T. Lagerwall, M.A. Osipov, S.A. Pikin, T. Sakurai, K. Yoshino, B. Zeks (Eds), Gordon & Breach, Philadelphia, PA (1991).
[16] D.M. Walba. In *Advances in the Synthesis and Reactivity of Solids*, Vol. 1, T.E. Mallouck (Ed.), JAI Press, Greenwich, CT (1991).
[17] M.A. Glaser, N.A. Clark, D.M. Walba, M.P. Keyes, M.D. Radcliffe, D.C. Snustad. *Liq. Cryst.*, **29**, 1073 (2002).
[18] M.A. Osipov, H. Stegemeyer, A. Sprick. *Phys. Rev. E*, **54**, 6387 (1996).
[19] D. Vizitiu, C. Lazar, B.J. Halden, R.P. Lemieux. *J. Am. chem. Soc.*, **121**, 8229 (1999).
[20] C.S. Hartley, C. Lazar, M.D. Wand, R.P. Lemieux. *J. Am. chem. Soc.*, **124**, 13513 (2002).
[21] C.J. Boulton, J.G. Finden, E. Yuh, J.J. Sutherland, M.D. Wand, G. Wu, R.P. Lemieux. *J. Am. chem. Soc.*, **127**, 13656 (2005).
[22] K. Miyasato, S. Abe, H. Takezoe, A. Fukuda, E. Kuze. *Jap. J. appl. Phys.*, **22**, L661 (1983).
[23] H. Stegemeyer, A. Sprick, M.A. Osipov, V. Vill, H.-W. Tunger. *Phys. Rev. E*, **51**, 5721 (1995).
[24] Y. Fuwa, K. Myojin, H. Moritake, M. Ozaki, K. Yoshino, T. Tani, K. Fujisawa. *Jap. J. appl. Phys.*, **33**, 5488 (1994).
[25] M. Ozaki, Y. Fuwa, K. Nakayama, K. Yoshino, T. Tani, K. Fujisawa. *Ferroelectrics*, **214**, 51 (1998).
[26] J. Goodby, E. Chin, J.M. Geary, J.S. Patel, P.L. Finn. *J. chem. Soc., Faraday Trans. 1*, **83**, 3429 (1987).
[27] A.F. Terzis, D.J. Photinos, E.T. Samulski. *J. chem. Phys.*, **107**, 4061 (1997).
[28] Although the methylene deuterons are formally diastereotopic, they are so far removed from the stereogenic centre in compounds **1** and **3** that they appear to be equivalent in isotropic solution.
[29] K. Czarniecka, E.T. Samulski. *Mol. Cryst. liq. Cryst.*, **63**, 205 (1981).
[30] J.W. Emsley, P. Lesot, J. Courtieu, D. Merlet. *Phys. Chem. chem. Phys.*, **6**, 5331 (2004); D. Merlet, A. Loewenstein, W. Smadja, J. Courtieu, P. Lesot. *J. Am. chem. Soc.*, **120**, 963 (1998); A. Meddour, I. Canet, A. Loewenstein, J.M. Péchiné, J. Courtieu. *J. Am. chem. Soc.*, **116**, 9652 (1994).
[31] K. Sakashita, T. Ikemoto, Y. Nakaoka, F. Terada, Y. Sako, Y. Kageyama, K. Mori. *Liq. Cryst.*, **13**, 71 (1993).
[32] S. Braun, H.-O. Kalinowski, S. Berger. *150 and More Basic NMR Experiments*. Wiley-VCH, Weinheim (1998).

Appendix

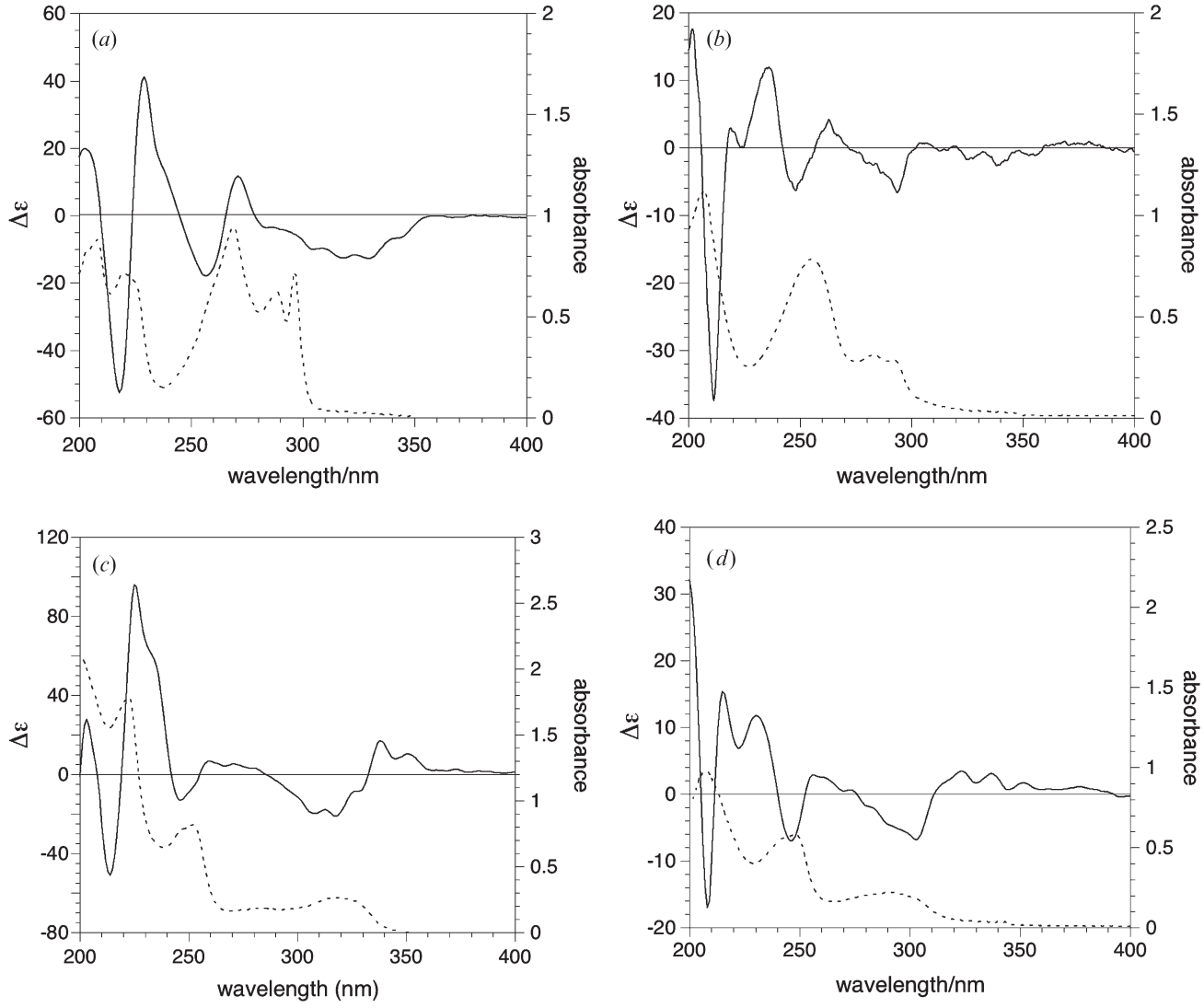

Figure A1. Circular dichroism (—) and UV–vis (—) absorption spectra of (a) dopant (*R*)-**1** (1.7×10^{-5}M), (b) dopant (*R*)-**2** (2.1×10^{-5}M), (c) dopant (*R*)-**3** (1.4×10^{-5}M), and (d) dopant (*R*)-**4a** (2.0×10^{-5}M) in hexanes.

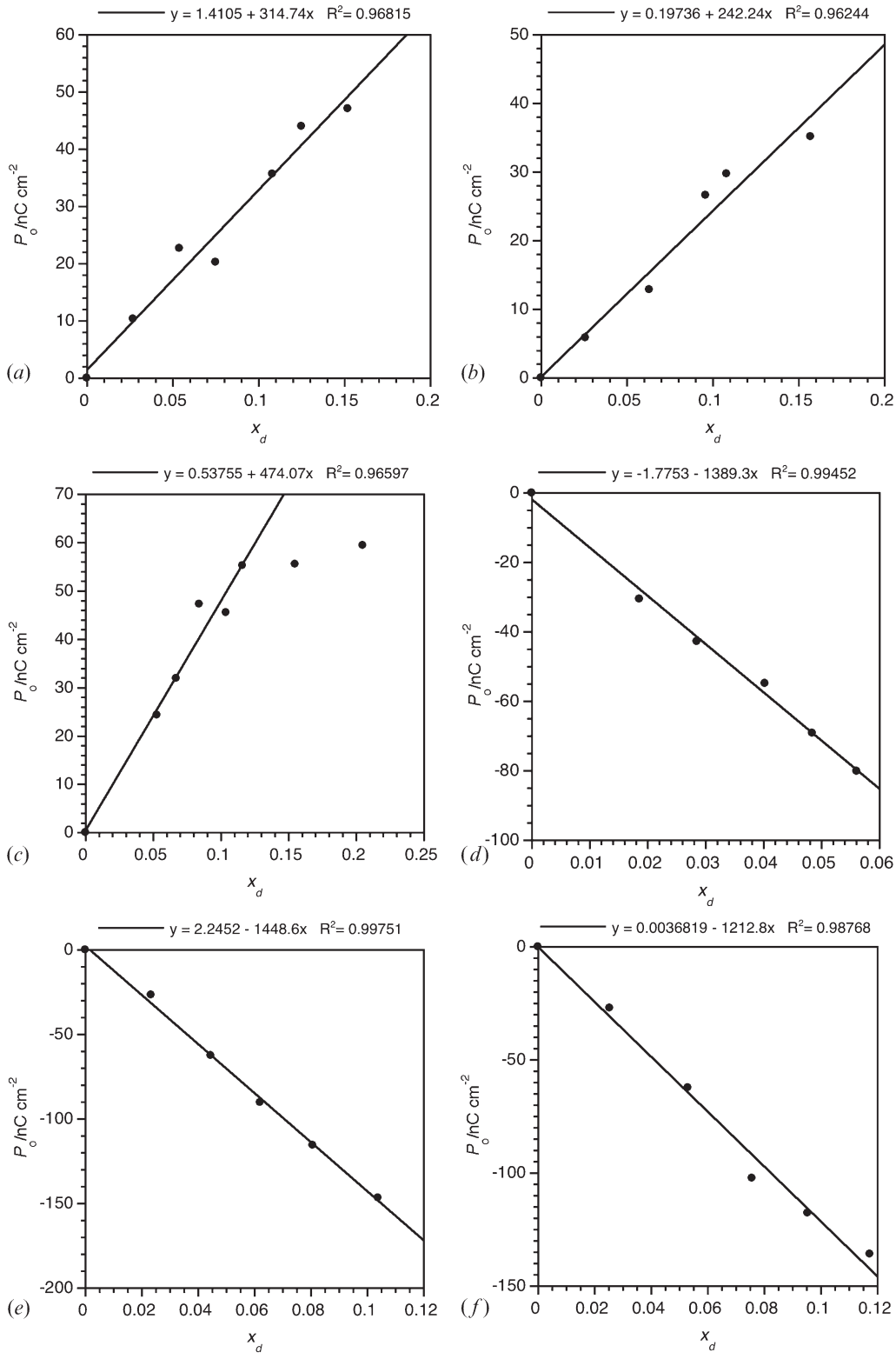

Figure A2. Reduced polarization P_o vs. dopant mole fraction x_d for dopant (*R*)-**2** in (a) **PhP**, (b) **PhBz**, (c) **NCB76**, and dopants (d) (*R*)-**4a** in **NCB76**, (e) (*R*)-**4b** in **NCB76** and (f) (*R*)-**4c** in **NCB76**. All measurements were performed at $T - T_C = -10$ K.